COMPEL - The international journal for computation and mathematics in electrical and electronic engineering

Particle transport in recirculated liquid metal flows
M. Kirpo, A. Jakovičs, B. Nacke, E. Baake,

Particle transport in recirculated liquid metal flows

M. Kirpo and A. Jakovičs
Laboratory for Mathematical Modelling of Environmental and Technological Processes, University of Latvia, Riga, Latvia, and

B. Nacke and E. Baake
Institute for Electrothermal Processes, University of Hannover, Hannover, Germany

Abstract

Purpose – Aims to present recent activities in numerical modeling of turbulent transport processes in induction crucible furnace.

Design/methodology/approach – 3D large eddy simulation (LES) method was applied for fluid flow modeling in a cylindrical container and transport of 30,000 particles was investigated with Lagrangian approach.

Findings – Particle accumulation near the side crucible boundary is determined mainly by the ρ_p/ρ ratio and according to the presented results. Particle settling velocity is of the same order as characteristic melt flow velocity. Particle concentration homogenization time depends on the internal flow regime. Separate particle tracks introduce very intensive mass exchange between the different parts of the melt in the whole volume of the crucible.

Originality/value – Transient simulation of particle transport together with LES fluid flow simulation gives the opportunity of accurate prediction of admixture concentartion distribution in the melt.

Keywords Particle physics, Simulation, Furnaces, Numerical analysis, Modelling

Paper type Research paper

Introduction

The liquid metal EM driven flow in the cylindrical container with two or more toroidal vortices of averaged flow is widely investigated because it is directly utilized in various industry applications. Induction crucible furnaces (ICF), cold crucible furnaces and EM stirrers can be mentioned as examples of such industrial facilities. The object of our interest is the particle tracing in ICF (Table I), which is filled with a Wood's melt ($\rho = 9{,}400\,\mathrm{kg/m^3}$, $\mu = 0.0042$ Pa s). The flow structure was previously investigated experimentally (Baake, 1994; Nacke *et al.*, 2006) and numerically (Baake *et al.*, 2003; Kirpo *et al.*, 2006).

The low-frequency velocity oscillations with the periods of order about 10 s were observed in this highly turbulent ($Re > 10^4$) melt flow during the experiments. Flow pulsations are very intensive in the interaction region of the upper and lower vortices and dramatically improve heat and mass exchange inside the crucible. There are proposed two reasons of the low-frequency oscillations:

Part of this work was carried out with the IBM pSeries supercomputer of the HLRN and the authors thank all members from the HLRN for their support. Also this work has been supported by the European Social Fund.

COMPEL: The International Journal for Computation and Mathematics in Electrical and Electronic Engineering
Vol. 27 No. 2, 2008
pp. 377-386

0332-1649
DOI 10.1108/03321640810847661

(1) instability of the whole flow (Taberlet and Fautrelle, 1985); and
(2) a continual creation and annihilation of large-scale vortices (Bojarevičs *et al.*, 2005), which is represented by several peaks in energy spectra.

These low-frequency pulsations are responsible for the melt temperature homogenization, which is very important for industrial applications. Another very important aspect of the metal production is melt alloying with admixtures (e.g. carbon), which is connected with their transport and homogenization.

Lagrangian approach was used to calculate particle positions in the melt at different time moments. Spherical particle motion was controlled only by the carrier fluid and by the external volumetric forces. Particles itself were not able to effect the flow pattern, hence one-way coupling was implemented. The number of tracked particles comparing to the fluid volume was small and collisions between particles were not taken into account. In such cases fluid flow can be calculated independently and then a new particle position can be established.

Numerical setup and verification of the hydrodynamic model

Experiments on Wood's melt velocity measurements in ICF (Figure 1) were performed. The turbulent metal flow is driven by the Lorentz forces that are excited by a symmetrical inductor, which height is equal to the liquid melt height or is 15 percent shorter. The developed averaged flow forms two toroidal vortices in the meridian plane, which are distributed symmetrically in respect to the crucible height (Figure 2(a)). The vortex structure is unstable and considering our experimental and numerical results can be observed only several seconds in the flow after EM field is switched on. Then the flow is divided into smaller turbulent vortices and the initial vortex structure can be reproduced only by averaging. Velocity measurements were performed using the permanent magnet probes (Ricou and Vives, 1982) and a digital data acquisition system. Maximal measured velocity in the melt was about 25 cm/s (Figure 2(a)) for $I = 2{,}000$ A, $f = 390$ Hz inductor current (Table I).

Turbulent energy maximum is placed near the crucible wall at a half-melt height where two averaged vortices are interacting (Figure 3). 2D axial-symmetric computer simulations show that two equation turbulent models often are not able to reproduce such turbulent energy distribution (Baake *et al.*, 2003). This may be caused by the turbulence isotropy hypothesis, which is used in two equation models. The flow

Table I.
Basic parameters of the ICF

Parameter	Symbol	Units	Value
Height of the melt	H	cm	57.0
Radius	R	cm	15.8
Height to diameter ratio	$H/(2R)$		1.8
Inductor current	I	A	2,000
Frequency	f	Hz	390
EM skin layer	δ	cm	2.5
Characteristic length	L	cm	15.8
Characteristic flow velocity	U	cm/s	10
Reynolds number	Re		3.5×10^4

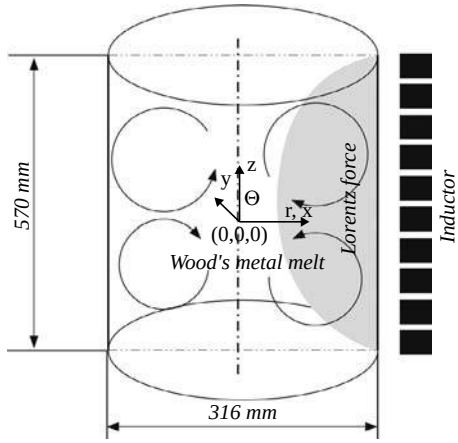

Figure 1.
Sketch of the experimental crucible

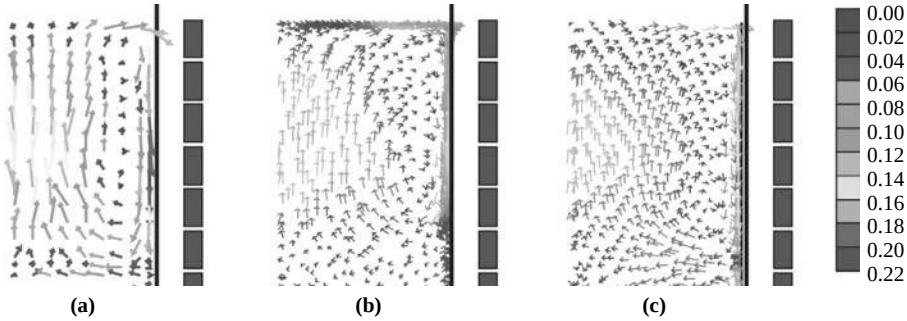

Figure 2.
The "main" vortices of the mean flow: (a) measured in experiments; (b) averaged LES with no-slip boundary conditions; (c) averaged LES with free slip boundary conditions

Note: Only top half of the cylindrical crucible is shown

turbulence in ICF is restricted by the crucible walls and by the flow vortex structure and in general it is not isotropic. Therefore, transient large eddy simulation (LES) turbulence model was used for numerical simulation.

Large turbulent scales are resolved directly while small scales (comparable with grid size) are simulated with the subgrid viscosity in LES. Reasonable results can be achieved even with the coarse grids but for the good accuracy and convergence Courant number ($Cr = U\delta t/\delta x$, where δt and δx are numerical time step and grid element size) should be below 1. The cylindrical crucible was meshed with 3 mm elements and had refined boundary layer near the side, top and bottom walls. All walls except free boundary in the top had no-slip conditions for the flow modeling (Figure 2(b)). However, particle tracing was performed with the model where free boundary conditions were also applied on the crucible walls (Figure 2(c)). The thickness of turbulent boundary layer is relatively small comparing to the 1 mm particles and we believe that this simplification is acceptable. LES calculations and unsteady particle tracing were performed in commercial CFD package Fluent with time step 0.005 s or 0.01 s. The converged 3D k-ε solution was used as initial conditions for the model, which represents the two main vortex flow in a meridian plane, i.e. without

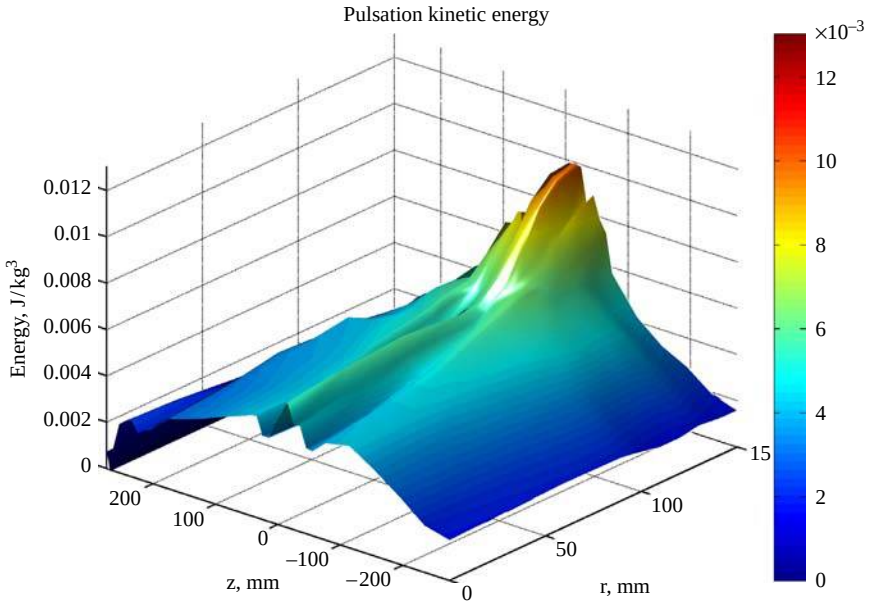

Figure 3.
Turbulent kinetic energy

angular velocity component. Another possible initialization option is to start with a zero velocity field at $t = 0$, which was performed in earlier calculations.

Calculated and measured data comparison introduces satisfied results. The structure of the flow is predicted very well with LES, while the absolute velocity values are closer to observed in the model with the free side boundary (Figures 2(a) and (c)).

Theoretical background and setup of particle tracing

The disperse particle motion in the conducting fluid under the influence of EM field is determined by several forces: Stokes drag force, buoyancy force, EM force and lift force, which is actually not included into the model. Particles in the wall-bounded turbulent flows are strongly affected by the flow structures and particle inertia, which is expressed as the preferential concentration of the particles (Eaton and Fessler, 1994). There is a lack of information on this phenomenon for complex flows, e.g. electromagnetically driven flow in a closed container (McKee *et al.*, 1999).

The Stokes number can be introduced to describe the intensity of the particle interaction with the fluid. It is defined as the ratio of the particle fluid response time constant to an appropriate turbulence time scale (dissipation time) and also it can be estimated as (Crowe, 2006):

$$St = \frac{\rho_p d_p^2 U}{18 \mu L}, \tag{1}$$

where ρ_p is the particle density, d_p is the particle diameter, μ is the dynamic viscosity, U and L are characteristic velocity and distance. Further, results correspond to $St \approx 0.1$ (Table II) with small variations depending on particle density. The next important parameter is dimensionless settling velocity:

$$\tilde{W} = \frac{1}{U}\,\frac{(\rho_p - \rho) g d_p^2}{18\mu}, \tag{2}$$

where g is gravitational acceleration. For selected particles (Table II) $\tilde{W} \approx 0.9$ and the problem should be mainly governing by the settling effects.

For particle transport simulation the next force balance equation was solved (Schiller and Naumann, 1933; Clift *et al.*, 1978):

$$\frac{d\vec{v}_p}{dt} = F_D(\vec{\mathbf{v}} - \vec{\mathbf{v}}_p) + \frac{\vec{\mathbf{g}}(\rho_p - \rho)}{\rho_p} + \vec{\mathbf{F}}_{pEM}, \quad F_D = \frac{18\mu}{\rho_p d_p^2}\left(1 + 0.15\,Re_p^{0.687}\right), \tag{3}$$

where particle Reynolds number Re_p is given by:

$$Re_p = \frac{\rho d_p \left|\vec{\mathbf{v}}_p - \vec{\mathbf{v}}\right|}{\mu}. \tag{4}$$

EM force influence on the spherical particle in homogeneous EM field can be derived solving Laplace equation for current density (Leenov and Kolin, 1954):

$$\vec{\mathbf{F}}_{pEM} = -\frac{3}{2}\,\frac{\sigma - \sigma_p}{2\sigma + \sigma_p}\,V_P \vec{\mathbf{f}}_{EM}, \tag{5}$$

where σ is the electrical conductivity, V_p is volume of the particle and the specific averaged electromagnetic Lorentz force is given by $\vec{\mathbf{f}}_{EM} = 0.5\,Re(\vec{\mathbf{j}} \times \vec{\mathbf{B}}^*)$. Equation (5) is a key for EM separation process, which can be used to remove impurities from the melt or to accumulate certain particles near the working boundary of the final product.

Surface injections of 30,000 particles ($d_p = 1$ mm) were placed on two orthogonal meridian planes ($x = 0$ and $y = 0$ in Cartesian coordinates, e.g. Figure 4(a), where this initial particle pattern is already disturbed by the angular flow perturbations). All particles were injected at $t = 0$ (i.e. at the start of transient simulation) and about 60 s of the flow were computed. In most simulations the difference between the particle and fluid densities was 1.1 times.

Modeling results

The initial flow structure on meridian plane computed by k-ε model is the same like the averaged LES solution (Figure 2). Velocity does not have angular components in a fully

Parameter	Symbol	Units	Value
Diameter	d_p	mm	1
Density	ρ_p	kg/m^3	8,545; 9,400; 10,340
Electrical conductivity	σ_p	1/(Ω m)	0
Number of injected particles	N		3×10^4
Stokes number	St		0.09
Particle Reynolds number	Re_p		<200
Dimensionless settling velocity	$\tilde{W}$		0.9

Table II. Physical properties of the injected particles

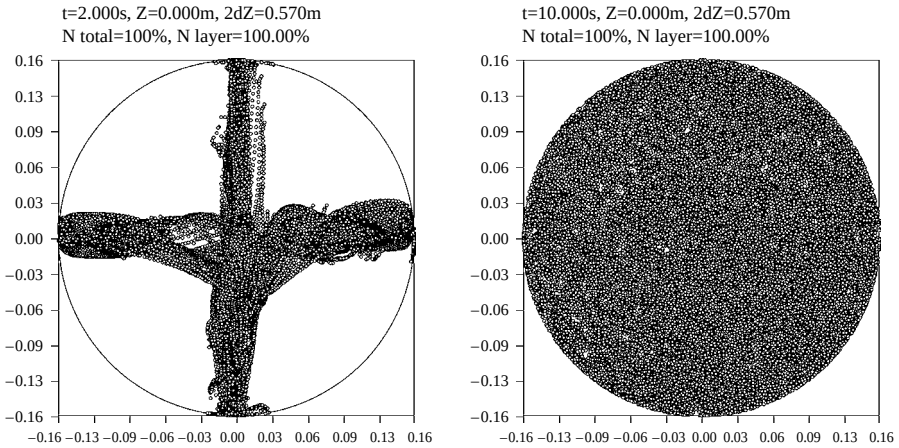

Figure 4.
Particle positions in the flow at different time moments, $\rho_p = \rho = 9{,}400\,\mathrm{kg/m^3}$

Notes: View from the top through the full crucible. Time is calculated from the particle injection. Particle tracking is performed starting from k–ε solution

converged k-ε solution and the angular homogenization of particle concentration is a result of 3D turbulent oscillations. The percent numbers in the chart captions (Figure 5) and on the right side of each chart represent a relative number of particles in the layer and a relative number of particles over the height, respectively. Changes in particle concentration can also be observed selecting thin boundary layer near the crucible wall and expanding this cylindrical layer over the angle (Figure 5). Angular and height distribution of particle is easily caught with this projection.

Particle density is equal to the fluid's density

In this case top and bottom directions are equivalent for the particles.

Flow perturbations start especially in the middle height between the averaged vortices, but also in the top and in the bottom parts of the crucible, where the melt flow is forced to change direction by the geometry or by the opposite coming flow. The middle zone of the near-wall boundary is also characterized by the presence of relatively large-scale vortices, which are long living. These vortices are created by the interaction of two near-wall jets coming from opposite directions. Instantaneous velocities can be high in this near-wall region but due to turbulent oscillations in average velocities tends to zero including radial component. Hence, these large-scale vortices are collinear to the wall and can accumulate particles inside, forming particle clusters. As a result, a zone of a slightly larger concentration can be located between the main vortices at a later time (Figure 5, middle), while the particle distribution over the height and over the angle in other parts of the layer is more or less uniform if particle and fluid densities are equal. Particle accumulation between the main vortices in the melt is also noticed in industrial ceramic crucibles, where oxide slag sediments are observed on the crucible walls.

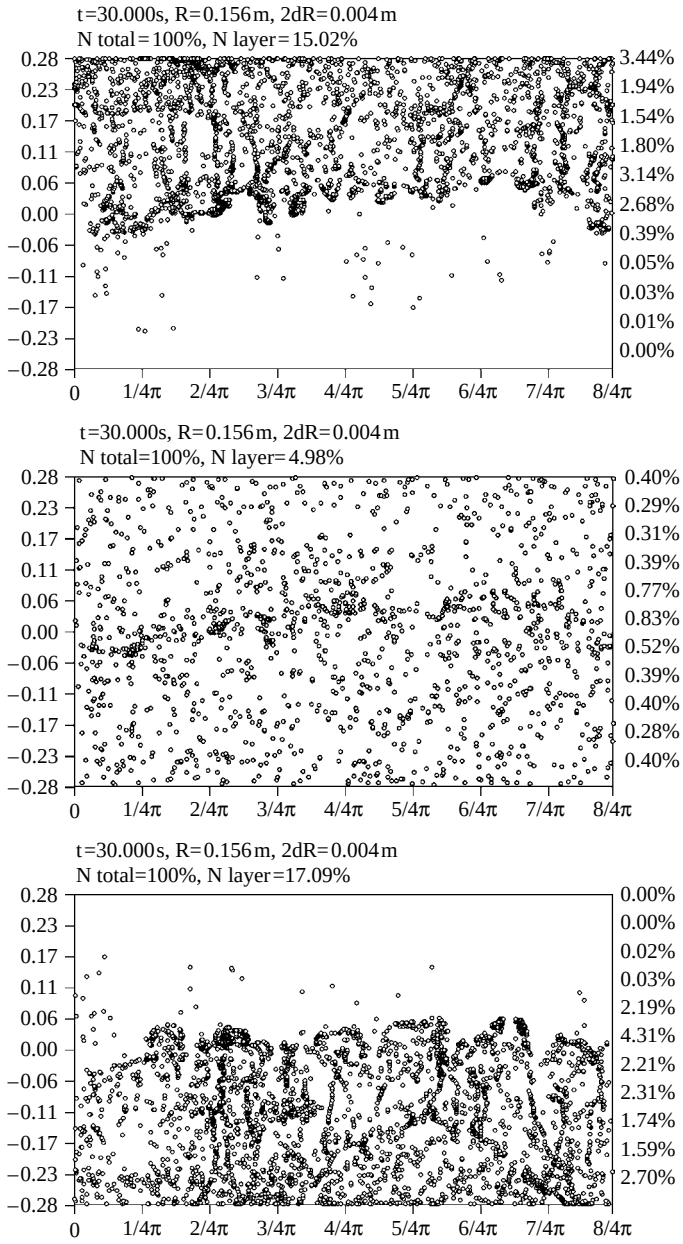

Note: View from the outside of the crucible

Figure 5.
Angular particle distribution in 4 mm thick layer near the side crucible wall and inside the melt at $t = 30$ s, $\rho_p = 8{,}545\ \text{kg/m}^3$ (top), $\rho_p = 9{,}400\ \text{kg/m}^3$ (middle), $\rho_p = 10{,}340\ \text{kg/m}^3$ (bottom)

To get more quantitative data for analysis a particle volume fraction $\varepsilon_p = NV_p/V$ (N is number of particles) maps can be studied. These maps represent evolution of the local particle volume fraction in time over the radial distance (Figure 7). Angular particle distribution does not have a preferred direction.

The homogenization of the particle distribution over takes about 10 s if simulation is started from the k-ε solution. Simulation shows, that homogenization time for fully developed turbulent flow is shorter by a factor of two ($\sim$5 s) than for transitional flow from the k-ε solution. The homogenization time can be correlated with the turnover period of the main flow eddy, which is about $6 \div 7$ s for 0.1 m/s average flow velocity. The minimal homogenization time is smaller but for more secure particle mixing several turnover periods are needed.

Particle density is 1.1 times higher or less than the fluid's density

Different particle density has changed distribution of the particles in the 4 mm near wall region, where the particles are concentrated mainly in the top or bottom parts of the layer (Figure 5 top and bottom). Such particles distribution in the melt is developed for 10 s and later almost does not vary over the time. Particles in the bottom part near the wall are moving together with the melt upward and their trajectories are close to vertical lines. Particles in the middle are affected by the smaller vortices forming particle clusters, which can influence angular particle distribution.

Disappearing of the particles from the top part of the near-wall region (Figure 5 bottom) can be explained by the forces, which are acting on particles for $\rho_p > \rho$($\rho_p < \rho$ is analogous). Here, is a tendency for particles to flow downward because of gravity. In the top part of the crucible the melt flow tries to drag the particle upward near the symmetry axis, but the probability of such event is smaller than for downward drag. Then the particle is directed to the boundary region and goes down at a first chance due to gravitational interaction. In the bottom part particle goes up only when they are constrained by the geometry. This hypothesis possibly is confirmed by the particle distribution inside the melt, where the particles are placed much more uniformly over the height comparing to the near-wall region.

Particle behavior in the melt is determined by their velocities (Figure 6). If the particle density and fluid density are not equal, then the local Re_p can achieve values up to 200. Therefore, the drag term in the equation (2) becomes determinative for the particle motion. If $\rho_p < \rho$ then the velocities of the particles in downward flow can be $2 \div 3$ times smaller than in the upward flow (Figure 6 left) and large count of particles is placed on the top free surface, but the crucible bottom is free from the particles. The velocity magnitude of the heavier particles in the downward flow is again a little higher (Figure 6 right) than in the upward flow, because the gravity.

Evolution of the particle volume fraction in time (Figure 7) presents its fast homogenization ($t < 10$ s) in the interior of the melt, while the initial particle concentration near the crucible wall increases only if $\rho_p \neq \rho$. Depending on the particle fluid density ratio the accumulation of particles can be observed in the top or bottom half of the crucible (Figure 5). Initial peaks in the particle volume fraction are connected to the transfer of the large number of boundary particles to the middle part of the boundary region after the model release at $t = 0$. Later these peaks become less explicit and the volume fraction tends to its average value. However, during the flow transition

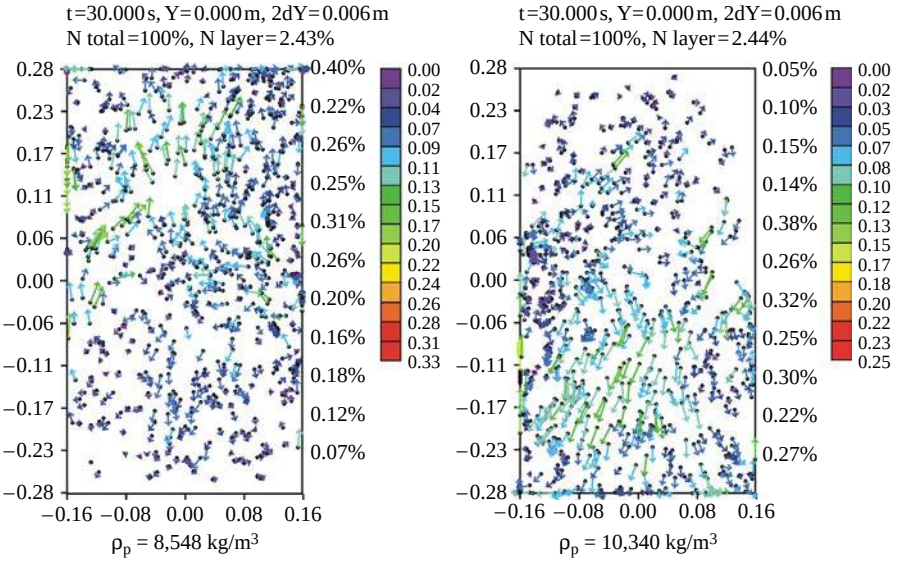

Figure 6.
Particle velocity pattern (m/s) in 6 mm thin meridian layer

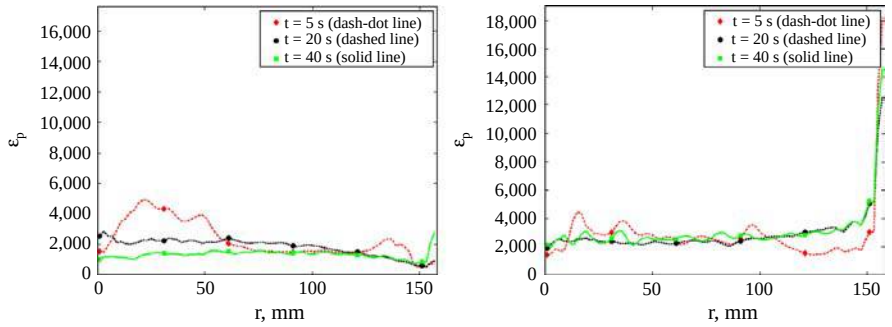

Figure 7.
Particle volume fraction ε_p evolution in time at different radiuses in bottom (left) and top part (right) of the crucible

Note: ρ_p = 8,545 kg/m^3

the particle concentration can have strong oscillations in the near-wall region, which period is correlated with the averaged eddy turn-over period.

Conclusions

Results of the Lagrangian particle tracing in the EM driven flow in the cylindrical container, which is like induction furnace, are presented. Particle volume fraction distribution evolution in time is studied for different particle densities.

Particle accumulation near the side crucible boundary is determined mainly by the ρ_p/ρ ratio and according to the presented results. Particle settling velocity is of the same order as characteristic melt flow velocity. Particle concentration homogenization time depends on the internal flow regime. Separate particle tracks introduce very intensive mass exchange between the different parts of the melt in the

whole volume of the crucible. Particle entrapment in the boundary region is caused by the sufficiently large local turbulent vortices with the restricted life time.

References

Baake, E. (1994), *Grenzleistungs und Aufkohlungsverhalten von Induktions-Tiegelöfen*, VDI, Düsseldorf.

Baake, E., Nacke, B., Umbrashko, A. and Jakovics, A. (2003), "Large eddy simulation modeling of heat and mass transfer in turbulent recirculated flows", *Magnetohydrodynamics*, Vol. 39 Nos 3/4.

Bojarevičs, A., Cramer, A., Gelfgat, Yu. and Gerbeth, G. (2005), "Experiments on the magnetic damping of an inductively stirred liquid metal flow", *Experiments in Fluids*, Vol. 40, pp. 257-66.

Clift, R., Grace, J.R. and Weber, M.E. (1978), *Bubbles, Drops and Particles*, Academic Press, New York, NY.

Crowe, C.T. (2006), *Multiphase Flow Handbook*, CRC Press, New York, NY.

Eaton, J.K. and Fessler, J.R. (1994), "Preferential concentrations of particles by turbulence", *Int. J. Multiphase Flow*, Vol. 20, pp. 169-209.

Kirpo, M., Jakovics, A., Baake, E. and Nacke, B. (2006), "Modeling velocity pulsations in a turbulent recirculated melt flow", *Magnetohydrodynamics*, Vol. 42, pp. 207-18.

Leenov, D. and Kolin, A. (1954), "Theory of electromagnetophoresis. I.Magnetohydrodynamic forces experienced by spherical & symmetrically oriented cylindrical particles", *Journ. of Chemical Phys.*, Vol. 22 No. 4, pp. 683-8.

McKee, S., Watson, R., Cuminato, J.A. and Moore, P. (1999), "Particletracking within turbulent cylindrical electromagneticallydriven flow", *Int. J. Numer. Meth. Fluids*, Vol. 29, pp. 59-74.

Nacke, B., Kirpo, M. and Jakovics, A. (2006), "LES study of flow characteristics in induction furnaces", *Proceedings of EPM2006*, Vol. 41, pp. 199-210.

Ricou, R. and Vives, C. (1982), "Local velocity and mass transfer measurements in molten metals using an incorporated magnet probe", *Int. Journal of Heat Mass Transfer*, Vol. 25, pp. 1579-88.

Schiller, L. and Naumann, Z. (1933), "Uber die grundlegenden Berechnungen bei der Schwerkraftaufbereitung", *Ver. Deut. Ing.*, Vol. 77, pp. 318-20.

Taberlet, E. and Fautrelle, Y. (1985), "Turbulent stirring in an experimental induction furnace", *J. Fluid Mech.*, Vol. 159, pp. 409-31.

Corresponding author
M. Kirpo can be contacted at: Maksims.Kirpo@lu.lv

This article has been cited by:

1. P.A. Oborin, S.Y. Khripchenko. 2013. Study of liquid metal flow and passive impurity transport driven by a traveling magnetic field in a rectangular cavity. *Computational Continuum Mechanics* **6**:2, 207-213. [CrossRef]